Saccharide-derived microporous spherical biochar prepared from hydrothermal carbonization and different pyrolysis temperatures: Synthesis, characterization, and application in water treatment

Hai Nguyen Tran[a]*, Chung-Kung Lee[b], Tien Vinh Nguyen[c], and Huan-Ping Chao[a]*

[a]*Department of Environmental Engineering, Chung Yuan Christian University, Chungli 320, Taiwan;* [b]*Department of Environmental Engineering, Vanung University, Chung-Li, 32061, Taiwan;* [c]*Faculty of Engineering and IT, University of Technology, Sydney (UTS), PO Box 123, Broadway, Sydney, Australia*

*Corresponding authors:

Emails: hpchao@cycu.edu.tw (H-P. Chao) and trannguyenhai2512@gmail.com (H.N. Tran)

Department of Environmental Engineering, Chung Yuan Christian University, Chung-Li, 32023, Taiwan, ROC.

Tel.: (886)-3-2654914

Saccharide-derived spherical biochar prepared from hydrothermal carbonization process anddifferent pyrolysis temperatures: Synthesis, characterization, and application in water treatment

Abstract

Three saccharides (glucose,sucrose, and xylose) were used as pure precursors for synthesizing spherical biochars (GB, SB, and XB), respectively. The two-stage synthesis process comprised:(1) the hydrothermal carbonization of saccharides to produce spherical hydrochar' and (2) pyrolysis of the hydrochar at different temperatures from 300 °C to 1,200°C. The results demonstrated that the pyrolysis temperaturesinsignificantly affected the spherical morphology and surface chemistry of biochar. The biochar' isoelectric point ranged from 2.64 to 3.90(abundant oxygen-containingfunctionalities). The Brunauer–Emmett–Teller (BET) specific surface areas (S_{BET}) and total pore volumes (V_{total}) of biochar increased with the increasing pyrolysis temperatures. The highest S_{BET} and V_{total} were obtained at a pyrolysis temperature of 900 °C for GB (775 m^2/g and 0.392 cm^3/g), 500 °C for SB (410 m^2/g and 0.212 cm^3/g), and 600 °C for XB (426 m^2/g and 0.225 cm^3/g).The spherical biochar was a microporous material with approximately 71%–98%micropore volume.X-ray diffraction results indicated that the biochar'structure was predominantly amorphous.The spherical biochar possessed the graphite structure when the pyrolysis temperature was higher than 600 °C. The adsorption capacity of GB depended strongly on the pyrolysis temperature. The maximum Langmuir adsorption capacities (Q^o_{max}) of 900GB exhibited the following selective order: phenol (2.332 mmol/g) > Pb^{2+} (1.052 mmol/g) > Cu^{2+} (0.825 mmol/g) > methylene green 5 (0.426 mmol/g) > acid red 1 (0.076 mmol/g). This study provides a simple method to prepare spherical biochar—a new and potential adsorbent for adsorbing heavy metals and aromatic contaminants.

Keywords: spherical biochar; saccharide; pyrolysis temperature; adsorption; heavy metal; aromatic pollutant.

1. Introduction

Biochar is a stable carbon-enriched and porous material, and it has been widely applied in soil amendment, water purification, and gas separation activities[1]. Biochar (also known as black carbon) can be produced through thermo-chemical conversion technology (pyrolysis). Pyrolysis—a dry carbonization process—is conducted at a high carbonization temperature (300–1,200 °C) in an inert atmosphere (i.e., N_2 or Ar atmosphere)[2], under vacuum conditions[3], or in non-circulated air atmosphere (i.e., within a lid-enclosed crucible)[4].

Generally, according to the literature, lignocellulose materials derived from agricultural wastes have been considered the most common feedstock for preparing biochar compared to other materials. Such feedstock comprised agricultural wastes and forest residues (rice husk, orange peel, sugarcane bagasse, hardwood, pine wood, and oak wood), industrial by-products (dairy manure, sewage sludge, anaerobically digested sugarcane bagasse, and anaerobically digested animal waste), and non-conventional materials (waste tyre rubber ash, paper, municipal solid waste, plastic, food waste, and bone char) [5-7]. However, biochar derived from the aforementioned feedstocks does not exhibit a spherical morphology. In water and wastewater treatment, biochar has attracted substantial attention because it typically possesses a relatively large specific surface area, high pore volume, well-developed porous structure, moderate cation exchange capacity, strong aromaticstructure, high thermal stability, and abundant surface oxygen-carrying functional groups (polar characters)[1, 5, 8]. However, applying such non-spherical biochar might be limited because it often containsa high level of impurities, total ash, and alkali and alkaline earth metallic contents.

In the literature, non-spherical biochar has been employed as a low cost and potential adsorbent for the removal of various contaminants in aqueous media, such as

Cu^{2+}, Pb^{2+}, As^{3+}, Cd^{2+}, Zn^{2+}, Cu^{2+}, Cr^{6+}, Hg^{2+}, PO_4^{3-}, phenol, naphthalene, fluridone, phenanthrene, nitrobenzene, methyl violet, malachite green, *p*–nitrotoluene, methylene blue, acid yellow 117, acid blue 25, methylene green 5, and rhodamine B [1, 8].

Many investigators have synthesized hydrochar spherical micro-sized particles (also known as spherical hydrochar or carbon sphere) derived from diverse organic materials (i.e., Polyvinylpyrrolidone, cellulose, glucose, xylose, starch, and sucrose) through hydrothermal carbonization process in a controlled temperature autoclave (150–350°C) for 2–48 h under a self-generated pressure[2, 9, 10].In addition, spherical activated carbon synthesized through chemical activation(using KOH [2, 9, 11], H_3PO_4 [12], NaOH [12], $ZnCl_2$[11],and the mixture of KOH and $ZnCl_2$ [11])and physical activation (using CO_2 [12] and steam [13]) has been reported in the literature. These spherical activated carbons were derived from pure glucose, sucrose, cellulose, furfural, starch, and xylose. However, the preparation process of spherical activated carbon always consumes more energy and requires further activation steps(chemical or physical activations). Therefore, the production cost of spherical activated carbon will be overwhelmingly higher than that of spherical biochar.

However, the preparation and characterization of spherical biochar have not yet been reported in the literature. Furthermore, previous investigations demonstrated that spherical activated carbon exhibits several enhanced characteristics, such as high wear resistance, high mechanical strength, superior adsorption, low impurity and ash content, smooth surface, high bulk density, high micropore volume, controllable pore size distribution, a high density of oxygen-containing functional groups when compared with the non-spherical activated carbon[10, 12, 14].

In this study,three pure saccharide precursors (glucose, sucrose, and xylose) was used to synthesize a newer spherical biochar compared to non-spherical biochar derived

from lignocellulose materials or non-conventional materials. The spherical biochar was synthesized through a two-stage process as follows: (1) a hydrothermal carbonizationat 190 °C under an autogenous pressure to produce spherical hydrochar; and (2) pyrolysis of the hydrocharat different temperatures in a laboratory scale reactorfor obtaining spherical biochar. The effects of pyrolysis temperatures from 300 °C to 11,00 °C on the spherical biochar's properties (i.e., textural, morphological, crystal, electrical, and adsorptive) were examined using various techniques. The spherical biochar was then applied to remove various pollutants from aqueous solutions. The target adsorbates in the study of adsorption isotherms comprised two heavy metals (copper and lead), phenol, one cationic dye (methylene green 5), and one anionic dye (acid red 1).

2. Materials and methods

2.1. Spherical biochar preparation

Three commercial saccharides, comprising one pentose (xylose) and two hexoses (glucose and sucrose), were selected as apure carbohydrate source. Spherical biochar was typically synthesized through the two-stage process. First, an aqueous glucose solution (150 mL, 1.5 M) is transferred into a 200-mL Teflon-lined autoclave. After a 24-h hydrothermal process at 190°C, the remaining brown precipitate particles (spherical hydrochar; GH) were separated using vacuum filtration, washed repeatedly with a 95% alcohol solution, and then abundantly washed with the distilled water until the pH of the filtrate reached 7.0. The hydrochar was then dried at 105°C for 12 h.

The second stage has been described as our recent study[7]. Approximately 20 g of the dried GHwas put into a porcelain crucible covered with a lid. The crucible was placed in a muffle furnace (Deng Yng DF 40, Taiwan) and subsequently pyrolyzed at different pyrolysis temperatures (from 300°C to 1,100°C) for 4 h in non-circulated air

atmosphere. The resulting black solid product, denoted as spherical biochar (GB),was washed repeatedly with an alcohol solution and distilled water until the pH value of the filtrate reached a constant value. Notably, the spherical biochars derived from xylose (XB) and sucrose(SB) were synthesised under the same conditions.

For convenience, the biochar samples were labelled according to pyrolysis temperature (°C). For example, glucose derived-spherical biochar (GB) samplesprepared from 300 °C to 1,100 °C were labelled300GB, 350GB, 400GB, 450GB, 500GB, 550GB, 600GB, 700GB, 800GB, 900GB, 1000GB, and 1100GB. The various hydrochar materials were denoted as follows: GH = glucose-derived hydrochar, XH = xylose-derived hydrochar, and SH = sucrose-derived hydrochar.The obtained adsorbents(spherical hydrochar and biochar) were stored in airtight brown bottles until required for use in the following experiments.

2.2. Characteristics of spherical biochar

The textural properties were measured by collecting nitrogen adsorption–desorption isotherms (Micromeritics ASAP 2020 sorptometer) at 77 K.The Brunauer–Emmett–Teller (BET) method was applied to calculate the specific surface area (S_{BET}; m^2/g).

$$S_{BET} = \frac{(0.1620 nm^2) \times (6.023 \times 10^{23})}{(22414 cm^3 STP) \times (10^{18} nm^2 / m^2) \times (S_1 + I_1)} \quad (1)$$

where 0.1260 nm^2 is the analysis gas (N_2) molecular cross-section area; 6.023 × 10^{23} isthe Avogadro'snumber; 22413 cm^3 is volume of 1 mole gas at standard temperature and pressure(STP);S_1(g/cm^3 STP) and I_1(g/cm^3 STP) are the slope (C-1/Q_{BET}×C) and intercept (1/Q_{BET} × C) of a plot of 1/Q(p^0/p-1) versus p/p^0(Equation 2), respectively; and the parameter $C$of the BET equationisobtainedusing Equation 3.

$$\frac{1}{Q(p^0/p-1)} = \frac{C-1}{Q_{BET}\times C}\, p/p^0 + \frac{1}{Q_{BET}\times C} \tag{2}$$

$$C = \frac{S_1 + I_1}{I_1} = \frac{1}{Q_{BET}\times I_1} \tag{3}$$

where Q is the quality adsorbed in volume (cm^3/g STP); C is an indicative of the energy of adsorption process (positive and dimensionless); $Q_{BET}$is a monolayer capacity in volume (cm^3/g STP); and p/p^0 is a relative pressure.

Similarly, the Langmuir surface area (S_{Lang}; m^2/g) was determinedusing Equation 4, the monolayer capacity in volume (Q_{Lang}; cm^3/g STP) was calculated from Equation 5, and the parameter b of the Langmuir equation was computed from Equation 6. Typically, in the same adsorbent, its S_{Lang} value must be higher than S_{BET} value.

$$S_{Lang} = \frac{(0.1620 nm^2)\times(6.023\times10^{23})}{(22414 cm^3 STP)\times(10^{18} nm^2/m^2)\times S_2} \tag{4}$$

$$Q_{Lang} = \frac{1}{S_2} \tag{5}$$

$$b = I_2 \times Q_{Lang} \tag{6}$$

$$\frac{P}{Q} = \frac{1}{Q_{Lang}} P + \frac{1}{b\times Q_{Lang}} \tag{7}$$

where S_2(g/cm^3 STP) and I_2 (g/cm^3 STP) are the slope ($1/Q_{Lang}$) and intercept ($1/b \times Q_{Lang}$) of a plot ofP/Q against P(Equation 7); P is an absolute pressure (kPa); and Q is the quality adsorbed in volume (cm^3/g STP) as defined in Equation 2.

External surface area (S_{ext}; m^2/g) and micropore volume (V_{mic}; cm^3/g) were calculated using the de Boer's *t*-plot (statistical thickness) method, withstatistic thickness*t* ranging from 3.5Å to 5.0 Å. Micropore surface area (S_{mic}; m^2/g) was

estimatedfrom the relationS_{mic} = S_{BET} (also known as total surface area) – S_{ext}. The thickness *t*(Å)can be computed bythe Halsey equation (Equation 10).

$$S_{ext} = \frac{S_3 \times (10^{10} A/m) \times D}{F \times (10^6 cm^3/m^3)} \tag{8}$$

$$V_{mic} = I_3 \times D \tag{9}$$

$$t = 3.54 \times [\frac{-5}{\ln(p/p^0)}]^{1/3} = 3.54 \times [\frac{5}{\ln(p^0/p)}]^{1/3} \tag{10}$$

where D is a density conversion factor (D = 0.0015468 cm^3 liquid/cm^3 STP); F is a surface area correction factor (F = 1.0); S_3(cm^3/g STP) and I_3 (cm^3/g STP) are the slopeand intercept of a plot of Q versus t, *respectively*.

Total pore volume (V_{total}; cm^3/g) and average pore diameter (L_o; nm) were estimated from equation; and characteristic adsorption energy (E_o; kJ/mol) was calculated from the Dubinin–Radushkevich equation.

$$V_{total} = \frac{Q_{0.99}}{647} \tag{11}$$

$$L_o = \frac{4 \times V_{toal}}{S_{BET}} \times 1000 \tag{12}$$

$$E_o = \frac{10.8}{L_o} + 11.4 \tag{13}$$

where$Q_{0.99}$ is the quality adsorbed in volume (cm^3/g STP) at the relative pressure (p/p^0) of 0.99.

Morphology and superficial element composition of spherical biochar were examined using scanning electron micros copy (SEM; Hitachi S-3000N, Japan). The morphologies and microstructures were determined using transmission electron microscopes with a 120-kV accelerating voltage (TEM; JEOLJEM-1230). The possible

crystalline structures were analysed using X-ray diffraction (XRD; PANalytical PW3040/60 X'Pert Pro). The functional groups present on the biochar's surface were detected using Fourier transform infrared spectroscopy (FTIR; FT/IR-6600 JASCO). A zeta potential analyser (Zetasizer 3000HS, Malvern Co.) measured the zeta potential of the various pH values of the spherical biochar samples.

Before analysing their characteristics, the spherical biochar and hydrochar were dried in a vacuum oven using N_2 gas at 105 °C for 12 h.

2.3. Isotherm adsorption experiment

In order to assess the adsorption characteristics of the synthesized spherical biochars and the effects of pyrolysis temperatures on their adsorption capacities, the adsorption isotherm of the biochar toward the test contaminants was conducted in batch experiments. Two metal ions (Pb^{2+} and Cu^{2+}) and three aromatic compounds [phenol, acid red 1 (AR1), and methylene green 5 (MG5)] were selected as typical adsorbates to determine the GB samples' adsorption characteristics. The chemical structures and basic properties of phenol, MG5, and AR1 are shown in Figure S1, and the basic and ionic properties of Cu^{2+} and Pb^{2+} are provided in Table S1.

Adsorption isotherms were conducted in various initial concentrations of the adsorbates: (0.48–4.83 mmol/L) for Pb^{2+}, (1.57–15.4 mmol/L) for Cu^{2+}, (2.13–10.6 mmol/L) for phenol, (0.39–1.96 mmol/L) for AR1, and (0.55–2.75 mmol/L) for MG5. Approximately 0.2 g of adsorbent (i.e., the spherical biochar or hydrochar) was subsequently added to 50 mL of aqueous adsorbate solution in a 100-mL Erlenmeyer flask. To prevent adsorption competition, only a single adsorbate was added in the flask. The adsorbent-adsorbate mixture was shaken using an orbital shaking incubator (S300R-Firstek) at 150 rpm and 30°C for 48 h. The solution pH was adjusted to 5.0 ± 0.2 before and during the adsorption experiment by adding 1 M NaOH or 1 M

HCl. One the adsorption process was completed, the mixture of solid and liquid was separated using glass fiber filters. The liquid was again filtered through a 0.45-μm syringe filter so that the concentration of the heavy metals could be examined.

The concentrations of phenol, MG5, and AR1 in the solution were determined using ultraviolent–visible spectrophotometry (Genesys 10 UV-Vis; Thermo Scientific) at maximum wavelengths of 265, 655, and 530 nm, respectively. Meanwhile, atomic absorption spectrometry (Avanta, GBC) was used to determine the concentrations of Pb^{2+} and Cu^{2+} ions in the solution. The amount of adsorbate uptake at equilibrium, q_e(mmol/g), was calculated using the mass balance equation, as follows:

$$q_e = \frac{(C_o - C_e)}{m} V \tag{14}$$

where C_o (mmol/L) and C_e (mmol/L) are the concentrations of the adsorbate at beginning and equilibrium, respectively; m (g) is the mass of adsorbent used; and V (L) is the volume of the adsorbate solution.

2.4. Statistical analysis and adsorption isotherm models

All adsorption experiments were conducted in duplicate, and the resulting data were averaged. If the bias of a repeated experiment exceeded 15%, a triplicate run was performed. Trial-and-error non-linear methods were executed using the "*Solver add-in*" (Microsoft Excel) to compute the parameters of the isotherm models. The coefficient of determination (R^2) of the non-linear optimization technique was computed using Eq. 15.

The effects of pyrolysis temperature on the maximum adsorption capacity of the test contaminants (Q^o_{max}) on biochar were statistically analysed using the Statgraphics Plus 3.0 statistical program. Differences were considered significant at p<0.01[15, 16].

$$R^2 = 1 - \frac{\sum (q_{e,\exp} - q_{e,cal})^2}{\sum (q_{e,\exp} - q_{e,mean})^2} \quad (15)$$

In this study, the Langmuir and Freundlich models were employed to describe the adsorptive behaviour of the adsorbate in the spherical hydrochar and biochar. The non-linear forms of the Langmuir and Freundlich equations are expressed in Equation 16 and Equation 17, respectively.

$$q_e = \frac{Q_{\max}^0 K_L C_e}{1 + K_L C_e} \quad (16)$$

$$q_e = K_F C_e^n \quad (17)$$

where q_e and C_e are obtained from Equation 1; Q^o_{max} (mmol/g) is the maximum saturated monolayer adsorption capacity of an adsorbent; K_L(L/mmol) is the Langmuir constant related to the affinity between an adsorbent and adsorbate; K_F [(mmol/g)/(mmol/L)^n]is the Freundlich constant, which characterizes the strength of adsorption; n (dimensionless; $0<n<1$) is a Freundlich intensity parameter, which indicates the magnitude of the adsorption driving force or surface heterogeneity. The adsorption isotherm is linear when $n = 1$, favourable when$n< 1$, and unfavourable when$n>1$.

All chemicals used in this study were or analytical grade.

3. Results and discussion

3.1. Characteristics of spherical biochar

3.1.1. Effect of pyrolysis temperature on textural properties

The nitrogen adsorption/desorption isotherms of the spherical biochars are presented in Figure 1(for GB) and Figure S2 (for XB and SB). According to the classification of gas physical adsorption isotherms (Figure S3) of the IUPAC, the adsorption isotherms of the spherical biochar belong to Type I of the IUPAC classification, and the Type I

isotherm is a typical characteristic of micropores (pore widths < 2 nm) with a small external surface area. This is well consistent with the textural properties of the spherical biochar samples prepared from 400 °C to 1,100 °C (Tables 1–2); their micropore and external surface areas ranged from 85 to 715 m^2/g and from 2.4 to 60 m^2/g, respectively. In addition, their micropore volume accounted for 71.2%–98.9% of the total pore volume, signifying that the spherical biochar was a microporous material.An analogous result was obtained by other scholars [2, 17, 18]. The spherical biochar's microporous property can be further confirmed by the magnitude of the characteristic adsorption energy (E_0; kJ/mol) that was calculated according to the Dubinin–Radushkevich equation. The E_0values of the spherical biochars produced at pyrolysis temperatures from 400°C to 1,100°C excessed 16 kJ/mol (Tables 1–2) as expected for microporous materials[2].

Figure 1

The effects of pyrolysis temperatures on textural parameters of the spherical biochar are presented in Tables 1–2. The spherical hydrochar samples possess low S_{BET} (0.985–7.08 m^2/g) and V_{total} (0.003–0.011 cm^3/g); however, afterundergoing the pyrolysis process at high carbonization temperatures, theirporositywas remarkably enhanced. Generally, the S_{BET} and V_{total} values of the biochars simultaneously increased with the increasing pyrolysis temperatures (Tables 1–2). When the pyrolysis temperatures are generally lower than 500°C, the spherical biochars exhibit poor porosity properties, which is consistent with the non-spherical biochars reported in the literature (Figure 2). However, when the pyrolysis temperatures exceed 500°C, the spherical biochars exhibit excellent porosity properties better than the non-biochars (Figure 2 and Table S2). As reported in the literature (Table S2), the S_{BET} surface areas(average ± SD) of non-spherical biochar were 5.72 m^2/g ± 7.22 (prepared at 300

°C), 13.09 ± 20.27 (350 °C), 38.99 ± 55.91 (400 °C), 26.14 ± 57.43 (450 °C),63.66 ± 78.75 (500 °C), 37.99 ± 44.87 (550 °C),12 0 ± 118(600 °C),185 ± 136(700 °C), 201 ± 174(800 °C), 227 ± 128 (900 °C), 224 ± 133(1,000 °C), and 167 ± 57 (1,100 °C).According to previous studies [19, 20], when the pyrolysis temperature was higher than 900 °C, the micropore structure of biochar collapsed, which results in a sintering effect, followed by a shrinkage of biochar and realignment of biochar structure.

The spherical biochar with large BET specific area and high pore volume is often expected to have excellent adsorption affinity towards various pollutants, while high micropore volume can coincide with its high adsorption capacity for nonionic organic compounds with small molecular sizes.

Table 1

Table 2

Figure 2

3.1.2. Morphology and crystal properties

The morphologies of the glucose-based biochar samples are illustrated in Figure 3 and Figure 4, and the morphology of the hydrochar samples is presented in Figure S4. The SEM images reveal interconnected spheres with relatively uniform sizes, smooth outer surfaces, regular spherical shapes, and high purity, while the TEM images demonstrate a porous structure with observed small pore sizes. Interconnected particle property of the biochar afforded more facile adsorbent separation from aqueous solutions (i.e., filtration with microfilter) because of an overall increase in particle size. Notably, the pyrolysis process did not sustainably affect the spherical morphologies of the samples, which means that both hydrochar and biochar samples exhibit the interconnected spheres in their morphologies (Figures 3–4 and Figures S4–S5).

Figure 3

Figure 4

According to Sevilla and Fuertes [21], the formation of the carbon-rich solid through the hydrothermal carbonization of glucose is attributed to dehydration, condensation, or polymerization and aromatization reactions. In essence, every spherical particle (carbon-rich solid) consists of two parts: firstly, a hydrophobic core comprising a condensed aromatic nucleus; and secondly, a hydrophilic shell (outer layer) comprising a high concentration of reactive oxygen functional groups, such as hydroxyl-phenolic, carbonyl, or carboxylic (Figure S6 and Figure 5) [21, 22].

The EDX spectra displayed in Figure 5 and Table S3 indicate that elements containing C and O are primary elements; for example, the spherical biochar is a carbon-rich solid that is approximately 73%–92% carbon for GB, 73%–98% for SB, and 75%–95% for XB. Thus, the spherical biochar can be classified as a carbonaceous microporous material. Noticeably, the content of oxygen on the spherical biochar's surface decreased sustainably with the increasing pyrolysis temperatures, suggesting that several oxygen-containing functional groups (i.e., –COOH and –OH) on the biochar's surface can be converted into CO, CO_2, or CO+CO_2 at higher pyrolysis temperatures [23].

Figure 5

XRD patterns of sphericalhydrochar and biochar are provided in Figure 6. Clearly, crystallinity structurewas not detected because of the absence of a sharp peak. As a result, the structures of sphericalhydrochar and biochar are completely amorphous.Moreover, two broad peaks at approximately $2\theta = 22°$ and 43° corresponded to the (002) and (100) planes of graphitic carbon materials, respectively.The layer distances of the (002) crystal plane ($d_{(002)}$; calculated from Equation 18) of spherical biochars prepared from pyrolysis temperatures from 700 to 1,100 °C were 0.417 and 0.389 (for the 700GB and 700XB

samples), 0.372 and 0.396 (800GB an 800XB), 0.401 and 0.395(900GB and 900XB), 0.376 and 0.389 (1000GB and 1000XB), and 0.407 and 0.386 (1100GB and 1100XB), respectively. Clearly, the $d_{(002)}$value of spherical biochar (0.372–0.417 nm) are larger than the corresponding value of graphite (0.3335 nm), suggesting that the carbon microspheres of biochar belong to an amorphous carbon mainly comprising the randomly oriented stacks of graphene sheets [24].

$$d = \frac{\lambda}{2\sin\theta} \tag{18}$$

whereλ= 0.154 nm for Cu $K\alpha$ radiation, and θ (degree) is the Bragg angle.

Notably, the spherical biochars prepared at 600 °C exhibited a small band with a Bragg diffraction peak at around 2θ = 19°, which belongs to the stacking structure of polymerized furan rings. However, this peak was shifted to a higher angle (approximately 23°) when the pyrolysis temperatures increased to 1,100 °C. Additionally, the intensity of two peaks at 2θ values of 22° and 43° increased pronouncedly when the pyrolysis temperatures were higher than 600 °C (Figure 6). The findingsconfirmed that (1) the graphite characteristics of spherical biochar were performed at a pyrolysis temperature higher than 600 °C, and (2) the structure of amorphous spherical biochar improved with increasing pyrolysis temperatures.

Figure 6

3.1.3. Surface chemistry

Qualitative information on the main functional groups present on the surface of the glucose-derived spherical biochar and their spectroscopic assignment is presented in Figure S7. The observed bands at approximately 3600 cm^{-1} are assigned to the (–OH) stretching vibrations of carboxylic acids, phenols, alcohols, or even absorbed water. The presence of carboxylic and lactonic groups (C=O) is evidenced by the well-defined

bands at roughly 1690 cm^{-1}. Similarly, the recognized bands at approximately 1520 cm^{-1} are ascribed to C=C double bonds in aromatic rings. Lastly, the presence of C−O groups is evident from the intense peaks at nearly 960 cm^{-1}[10, 21]. Noticeably, the intensity of the C=O and C–O groups decreased as the pyrolysis temperatures increased, suggesting that the oxygen-containing functionalities on the spherical biochars' surface can be destroyed at higher temperatures.

Similar to activated carbon, the oxygen-containing functional groups on the spherical biochar's surface can be classified into two main types: acidic group (i.e., carboxylic acid, lactone, and phenol groups) and basic group (i.e., chromene, pyrone, and quinoes) [25].This means that the spherical biochar typically coexists with both acidic and basic properties in solutions (amphoteric nature); and the dominant concentration of total acidic groups or total basic groups is strongly dependent on its isoelectric point (IEP) or point of zero charge (PZC)[26].

The electrical state of the surface adsorbents in solutions was characterized by both IEP and PZC. Figure 7 presents the Zeta potential (ζ) of the spherical hydrochar and biochar samples as a function of pH. The isoelectric point (pH_{IEP}) is defined as the conditions at which the electro-kinetic charge density and thus the electro-kinetic (ζ) potential equals zero [27]. The IEP values are only representative of the external surface charges of carbon particles in solutions whereas the PZC varies in response to the net total (external and internal) surface charge of the adsorbent[28]. However, both IEP and PZCpossibly serve as a useful indicator of the nature offunctionalities on the surface of carbonaceous materials (i.e., biochar and activated carbon) [25].

Figure 7

Essentially, a positive zeta potential indicates a positive surface charge on the external surface of adsorbent, and vice versa. The spherical hydrochar possesses a low

pH_{IEP} value (i.e, pH_{IEP} 2.75 for GH, 2.61 for SH, and 2.72 for XH), demonstrating that ample organic acids can be formed during the hydrothermal carbonization process. Clearly, the IEP values of the spherical biochar were insignificantly dependent on the pyrolysis temperatures. The IEP values slightly increased when the pyrolysis temperatures increased from 300°C to 1,100°C. Notably, the average pH_{IEP} of GB (3.310 ± 0.136), SB (3.311 ± 0.388), and XB (3.319 ± 0.432) prepared from 300 °C to 1,100 °C demonstrated identical results, suggesting that the pyrolysis temperatures and the saccharide precursors did not remarkably effect on the pH_{IEP} of spherical biochar.

According to these IEP values, the spherical biochar can be classified into the L-carbon (pH_{IEP}< 7.0) which possessesplentiful oxygen-carrying functional groups (i.e., carboxylic, phenolic, and lactone groups) acting as Brønsted acids [25, 29]. Furthermore, the zeta potential of GB at pH 5 ranged from –3.5 mV to –14.1 mV, indicating that its external surface is negatively charged at the solution pH of 5.0. Therefore, in this study, we adjusted solution pH to 5.0 during the adsorption experiments for two reasons: (1) avoiding the precipitation of the heavy metal ions and the dissociation of phenol; and (2) ensuring that the biochars' surface remained negative charges during the adsorption process.

3.2. Adsorption efficiency of heavy metals and aromatic contaminants

The adsorption isotherms of aromatic contaminants (i.e., MG5, AR1, and phenol) and potentially toxic metals (i.e., Pb^{2+} and Cu^{2+}) onto glucose-derived biochars developed from 600 °C to 900 °C are presented in Figure 8 and Figure 9, respectively. Obviously, the pyrolysis temperatures played a vital role in determining adsorption capacity of the spherical biochar toward the test contaminants. Adsorption capacities of the spherical biochar samples toward these contaminants exhibited the following order: 900GB > 800GB > 700GB > 600GB (p<0.01), which demonstrates that the increase in the

pyrolysis temperatures from 600°C to 900°C resulted in enhanced adsorption capacities of the spherical biochars for target heavy metals and aromatic contaminants. Furthermore, the adsorption capacity of the spherical biochar generally was overwhelmingly higher than that of it precursor (i.e., the spherical hydrochar). This is because the spherical biochar exhibits excellent porosity properties (i.e., BET specific surface area, and total pore volume shown in Table 1) compared to the spherical hydrochar (GH).

Figure 8

Figure 9

Table 3 and Table 4 display the corresponding isotherm parameters of the tested organic and inorganic contaminants, respectively. According to the coefficient of determination (R^2), it can be concluded that the adsorption equilibrium data can be better described by the Langmuir model (R^2= 0.91–0.99 for the adsorption of aromatic contaminants; and R^2= 0.95–0.99 for the adsorption of heavy metals) than the Freundlich model (R^2= 0.82–0.99; and R^2 = 0.86–0.98), respectively. This conclusion agrees well with the experimental data of adsorption equilibrium shown in Figures8–9. Clearly, the region in which the experimental data relating to the adsorption equilibrium are located is the Langmuir region, which is characterized by saturation at high concentrations.

Table 3

Table 4

For the removal of aromatic adsorbates, the maximum adsorption capacities (Q^o_{max}; mmol/g) of the spherical biochar samples calculated from the Langmuir model demonstrated a selective adsorption order of phenol > methylene green 5 > acid red 1. Firstly, this adsorptions order is in consistent with the molar mass values of the

adsorbates in Figure S1, as follows: AR1 (509 g/mol) > MG5 (433 g/mol) > phenol (94 g/mol).

Phenol has a smaller molar mass than AR1 and MG5; therefore phenol molecules can easily penetrate the micropore of biochars. Consequently, the biochar samples exhibited relatively greater adsorption capacity for this adsorbate. An analogous result has been noted in other studies [9, 30]. They reported that phenol adsorption mainly occurs in micropores smaller than 1.4 nm, and the average pore width of the spherical biochar samplesprepared from 600 °C to 900 °C in this study was 1.93 nm to 2.02 nm (Table 1). Therefore, the micropore filling is a central mechanism of phenol adsorption onto the spherical biochar samples. The poorer adsorption capacity toward AR1 might be attributed to the repulsion interactions that occur between the negatively charged sites on the biochar's surface and the negatively charged AR1 molecules. The repulsion phenomenon can be supported by the isoelectric point (IEP) of the spherical biochar which is measured by the zeta potential (IEP ranging from 3.15 to 3.52; Figure 7). Similarly, Lee and colleagues [31] applied a mesoporous zeolite (MCM-41) to remove of two acid dyes (i.e., acid red 1 and erioglaucine) and three basic dyes (Rhodamine B, Crystal Violet, and Methylene Green 5). They concluded that the low adsorption capacity of two acid dyes compared to three basic dyes onto MCM-41 can be explained by the existence of repulsion forces.

Generally, the adsorption efficiencies ($Q^o_{\max}$; mmol/g) of Cu^{2+} onto the spherical biochar samples were remarkably higher than those of Pb^{2+} (Table 4). The adsorption amount order can be explained by the ions' chemical properties (i.e., hydrated ionic radius, ionic potential, electronegativity, charge density, first hydrolysis equilibrium constant, and ionic radius; Table S1). The Q^o_{max} values are inversely proportional to the hydrated ionic radius of the metals, in which $Pb^{2+} > Cu^{2+}$. In general, a metal with a

smaller hydrated ionic radius can easily pass through water clusters and penetrate smaller pores, resulting in greater access to the active sites on an adsorbent's surface [32]. However, the hydrated ionic radii of Pb (4.10 Å) and Cu (4.19 Å) are nearly the same, so they may not reflect the diverse adsorption capacities of Cu^{2+} and Pb^{2+}. Moreover, the ionic potential of Cu (approximately 2.73), defined as a quotient of ionic charge and ionic radius, is higher than that of Pb (approximately 1.68), indicating that the Cu ions have a higher affinity to oxygen functional groups on an adsorbent's surface than the Pb ions. Furthermore, Cupossesses greater electronegativity (approximately 2.0), charge density ($13.6 \times 10^9 C/m^3$), and first hydrolysis equilibrium constant (pK = approximately 7.9) than did Pb (approximately 1.87, $4.30 \times 10^9 C/m^3$, and pK = 7.7, respectively). This indicates that it also has stronger electrostatic attractions and a higher affinity for adsorption sites on an adsorbent. The smaller ionic radius of Cu (approximately0.73Å) compared with Pb (approximately1.19Å) also suggests that more Cu ions can be adsorbed by the adsorbent's surface[33].

The Gibbs energy change (ΔG°) was calucaletd according to the laws or thermocynamic using Equation 19 [15, 16]. As expected, the Gibbs energy change exhibits a negative value (Table 3 and Table 4), which indicates that the adsorption process of test contaminants onto the spherical hydorchar and biochar samples occur spontaneously in operating conditions. Additionally, the Freundlich exponent n is lower than 1, indicating that the shape of test adsorbates' isotherms is favorable.

$$\Delta G^o = -RT \ln K_C \tag{19}$$

where R is the universal gas constant (8.3144 J/(mol × K)) and T is the absolute temperature in Kelvin, and K_C is the equilibrium constant (dimensionless). K_C can be easily obtained as a dimensionless parameter by multiplying K_L by 55.5 [the number of moles of pure water per liter (1,000 g/L divided by 18 g/mol)] and then by 1,000.

For comparison, in similar operating conditions (i.e., the initial solution pH, temperatures, shaking speed, etc.), the spherical biochar samples exhibit similar adsorption capacities of cationic dye, phenol, lead, and copper to the commercial activated carbon (Table 3 and Table 4). Given that it has favorable textural properties, surafce chemistry, and excellent adsorption capacity, the spherical biochar can be regarded as a green and renewable materialable to remove industrialwastewater effluents.

4. Conclusions

The study proposed an approach towards advanced carbon synthesis based on renewable resources. The newer spherical biochars prepared from glucose, sucrose, and xylose through the pre-hydrothermal process exhibit a smooth spherical morphology. Their textural properties did strongly depend on the pyrolysis temperatures. The BET surface areas and total pore volumes of the spherical biochars increased significantly when the pyrolysis temperature was higher than 500°C. The glucose-derived spherical biochar produced at 900°C exhibited the highest BET surface area (775 m^2/g) and total pore volume (0.392 cm^3/g). The spherical biochars exhibited abundant oxygen-containing surface functional groups on their surface.

The maximum adsorption capacities (Q^o_{max}) of the glucose-derived spherical biochars towards various tested contaminants were determined from the Langmuir model; the Q^o_{max} values increased whenthe pyrolysis temperature also increased (p<0.01). The 900GB sample possessed the highest $Q^o_{max}$with the selective order of phenol (2.332 mmol/g) > Pb^{2+} (1.052 mmol/g) > Cu^{2+} (0.825 mmol/g) > methylene green 5 (0.426 mmol/g) >acid red 1 (0.076 mmol/g).

It was experimentally concluded that the spherical biochar is an environmentally friendly adsorbent that demonstrates much potential in removing dangerous contaminants from the environment.

Acknowledgements

This current work was financially supported by Chung Yuan Christian University (CYCU) in Taiwan. The first author would like to thank Chung Yuan Christian University for the Distinguished International Graduate Students (DIGS) scholarship to pursue his doctoral studies.

References

1.Joseph, S. and J. Lehmann, *Biochar for environmental management: science and technology*. 2009: London, GB: Earthscan.

2.Sevilla, M., A.B. Fuertes, and R. Mokaya, *High density hydrogen storage in superactivated carbons from hydrothermally carbonized renewable organic materials.* Energy & Environmental Science, 2011. **4**(4): p. 1400-1410.

3.Ismadji, S., et al., *Activated carbon from char obtained from vacuum pyrolysis of teak sawdust: pore structure development and characterization.* Bioresource Technology, 2005. **96**(12): p. 1364-1369.

4.Tran, H.N., S.-J. You, and H.-P. Chao, *Fast and efficient adsorption of methylene green 5 on activated carbon prepared from new chemical activation method.* Journal of Environmental Management 2017. **188**: p. 322-336.

5.Inyang, M.I., et al., *A review of biochar as a low-cost adsorbent for aqueous heavy metal removal.* Critical Reviews in Environmental Science and Technology, 2016. **46**(4): p. 406-433.

6.Tripathi, M., J.N. Sahu, and P. Ganesan, *Effect of process parameters on production of biochar from biomass waste through pyrolysis: A review.* Renewable and Sustainable Energy Reviews, 2016. **55**: p. 467-481.

7.Tran, H.N., S.-J. You, and H.-P. Chao, *Effect of pyrolysis temperatures and times on the adsorption of cadmium onto orange peel derived biochar.* Waste Management & Research, 2016. **34**(2): p. 129-138.

8.Mohan, D., et al., *Organic and inorganic contaminants removal from water with biochar, a renewable, low cost and sustainable adsorbent – A critical review.* Bioresource Technology, 2014. **160**: p. 191-202.

9.Huang, F.-C., et al., *Preparation of activated carbon using micro-nano carbon spheres through chemical activation.* Journal of the Taiwan Institute of Chemical Engineers, 2014. **45**(5): p. 2805-2812.

10. Jain, A., R. Balasubramanian, and M.P. Srinivasan, *Hydrothermal conversion of biomass waste to activated carbon with high porosity: A review.* Chemical Engineering Journal, 2016. **283**: p. 789-805.

11. Härmas, M., et al., *Microporous–mesoporous carbons for energy storage synthesized by activation of carbonaceous material by zinc chloride, potassium hydroxide or mixture of them.* Journal of Power Sources, 2016. **326**: p. 624-634.

12. Romero-Anaya, A.J., et al., *Spherical carbons: Synthesis, characterization and activation processes.* Carbon, 2014. **68**: p. 296-307.

13. Yang, Y., et al., *Preparation and antibacterial properties of an activated carbon sphere-quaternary phosphonium salt composite.* RSC Advances, 2014. **4**(92): p. 50708-50712.

14. Titirici, M.-M., et al., *Black perspectives for a green future: hydrothermal carbons for environment protection and energy storage.* Energy & Environmental Science, 2012. **5**(5): p. 6796-6822.

15. Tran, H.N., S.-J. You, and H.-P. Chao, *Thermodynamic parameters of cadmium adsorption onto orange peel calculated from various methods: A comparison study.* Journal of Environmental Chemical Engineering, 2016. **4**(3): p. 2671-2682.

16. Tran, H.N., et al., *Mistakes and inconsistencies regarding adsorption of contaminants from aqueous solutions: A critical review.* Water Research, 2017. **120**: p. 88-116.

17. Tooming, T., et al., *High power density supercapacitors based on the carbon dioxide activated d-glucose derived carbon electrodes and 1-ethyl-3-methylimidazolium tetrafluoroborate ionic liquid.* Journal of Power Sources, 2015. **280**: p. 667-677.

18. Tran, H.N., et al., *Activated carbon derived from spherical hydrochar functionalized with Triethylenetetramine: synthesis, characterizations, and adsorption application*, in *Green Processing and Synthesis*. 2017.

19. Brown, R.A., et al., *Production and characterization of synthetic wood chars for use as surrogates for natural sorbents.* Organic Geochemistry, 2006. **37**(3): p. 321-333.

20. Guo, J. and A. Chong Lua, *Characterization of chars pyrolyzed from oil palm stones for the preparation of activated carbons.*

Journal of Analytical and Applied Pyrolysis, 1998. **46**(2): p. 113-125.

21. Sevilla, M. and A.B. Fuertes, *Chemical and structural properties of carbonaceous products obtained by hydrothermal carbonization of saccharides.* Chemistry - A European Journal, 2009. **15**(16): p. 4195-4203.

22. Sevilla, M. and A.B. Fuertes, *The production of carbon materials by hydrothermal carbonization of cellulose.* Carbon, 2009. **47**(9): p. 2281-2289.

23. Figueiredo, J.L., et al., *Modification of the surface chemistry of activated carbons.* Carbon, 1999. **37**(9): p. 1379-1389.

24. Xu, S., et al., *Alkali-assisted hydrothermal route to control submicron-sized nanoporous carbon spheres with uniform distribution.* Colloids and Surfaces A: Physicochemical and Engineering Aspects, 2017. **515**: p. 1-11.

25. Bandosz, T.J. and C.O. Ania, *Chapter 4 Surface chemistry of activated carbons and its characterization.* Interface Science and Technology, 2006. **7**: p. 159-229.

26. Tran, H.N., S.-J. You, and H.-P. Chao, *Activated Carbons from Golden Shower upon Different Chemical Activation Methods: Synthesis and Characterizations.* Adsorption Science & Technology, 2017.

27. Kosmulski, M., *Surface charging and points of zero charge*. Vol. 145. 2009: CRC Press.

28. Onjia, A.E. and S.K. Milonjić, *Influence of the background electrolyte on the point of zero charge of chromium(III)-oxide*, in *Materials Science Forum*. 2002. p. 87-92.

29. Mattson, J.S. and H.B. Mark, *Activated carbon: surface chemistry and adsorption from solution*. 1971, New York: M. Dekker.

30. Lorenc-Grabowska, E., G. Gryglewicz, and M.A. Diez, *Kinetics and equilibrium study of phenol adsorption on nitrogen-enriched activated carbons.* Fuel, 2013. **114**: p. 235-243.

31. Lee, C.-K., et al., *Application of MCM-41 for dyes removal from wastewater.* Journal of Hazardous Materials, 2007. **147**(3): p. 997-1005.

32. Petrov, N., T. Budinova, and I. Khavesov, *Adsorption of the ions of zinc, cadmium, copper, and lead on oxidized anthracite.* Carbon, 1992. **30**(2): p. 135-139.

33. Haynes, W.M., *CRC handbook of chemistry and physics*. 2014: CRC press.

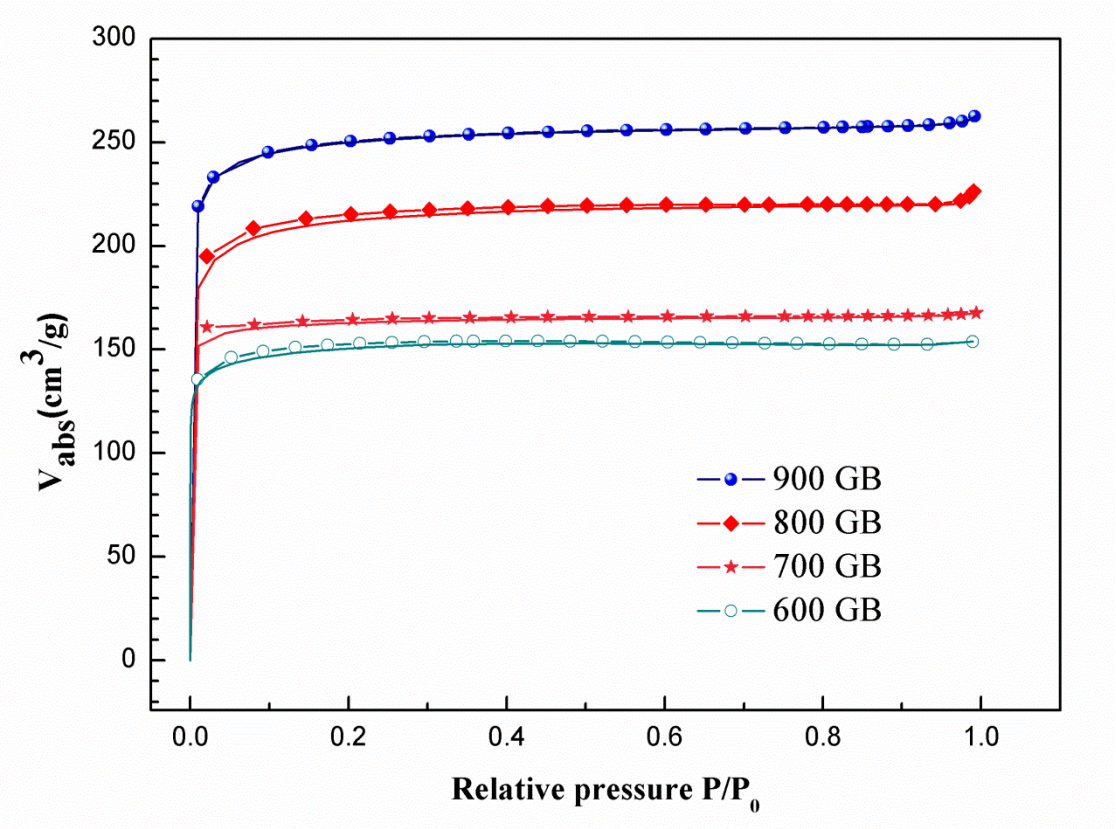

Figure 1. Nitrogen adsorption/desorption isotherms of glucose-derived spherical biocharsprepared from different pyrolysis temperatures (600–900°C).

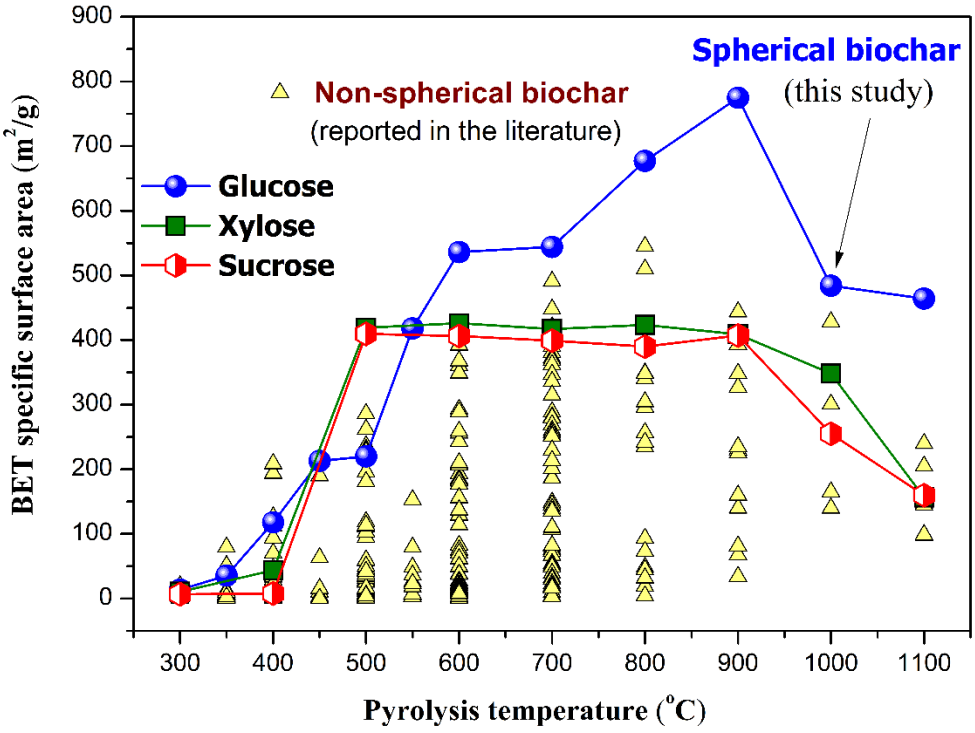

Figure 2. Comparison of BET specific surface area of spherical biochar in this study and non-spherical biocharreported in the literature.

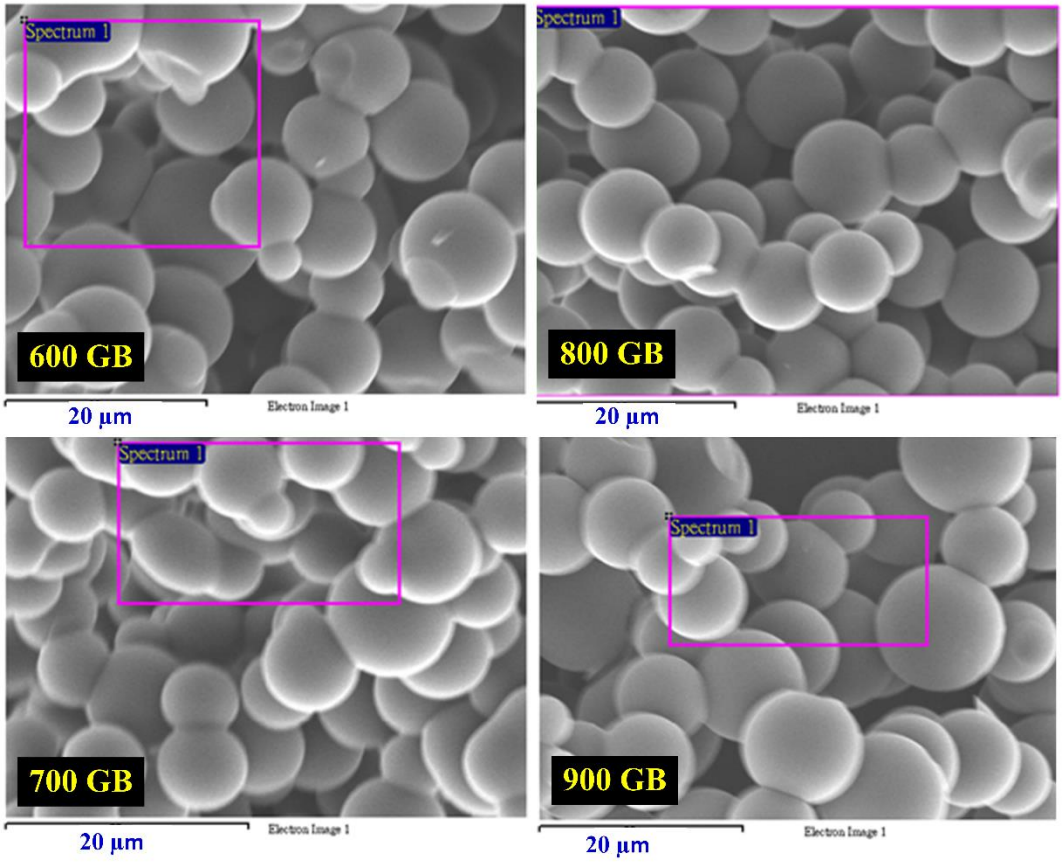

Figure 3. SEM images of glucose-derived spherical biochars produced from different pyrolysis temperatures (600–900 °C).

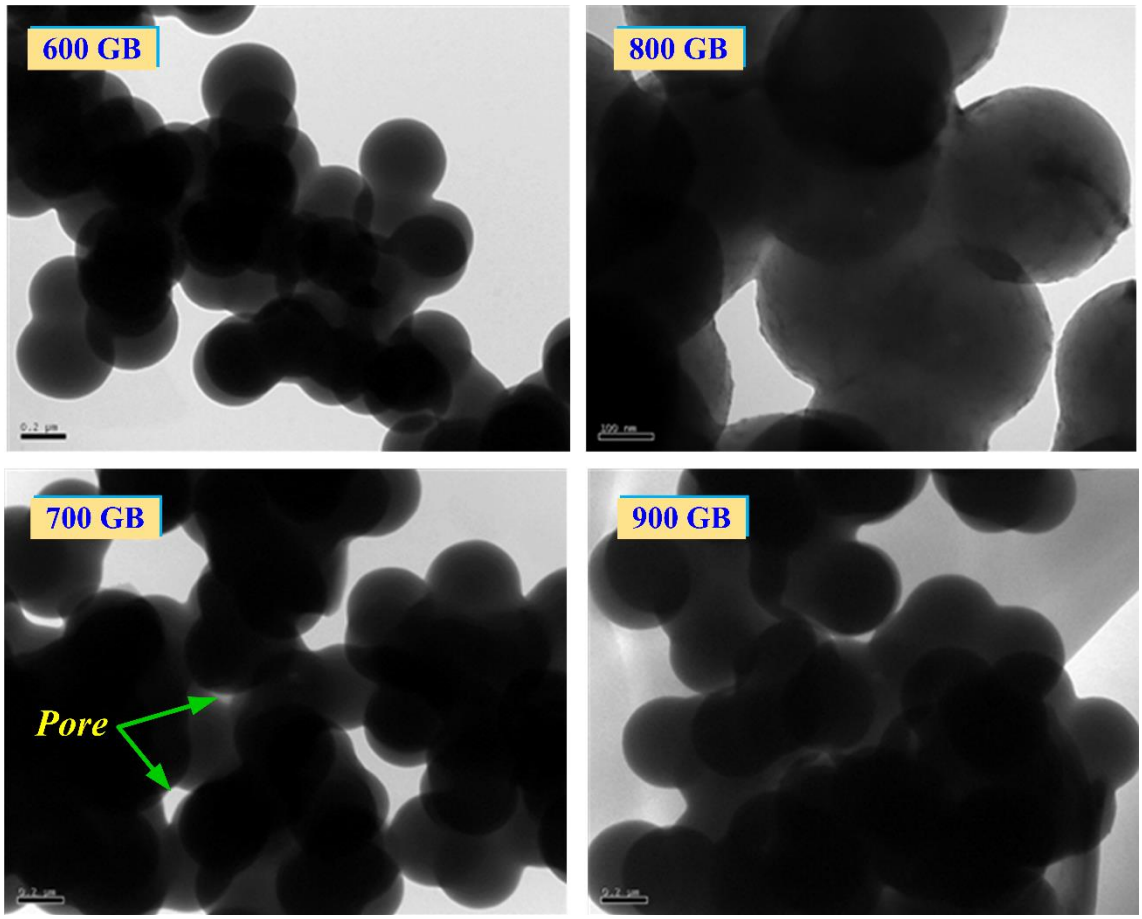

Figure 4. TEM imagesofglucose-derived spherical biochars produced from different pyrolysis temperatures (600–900 °C).

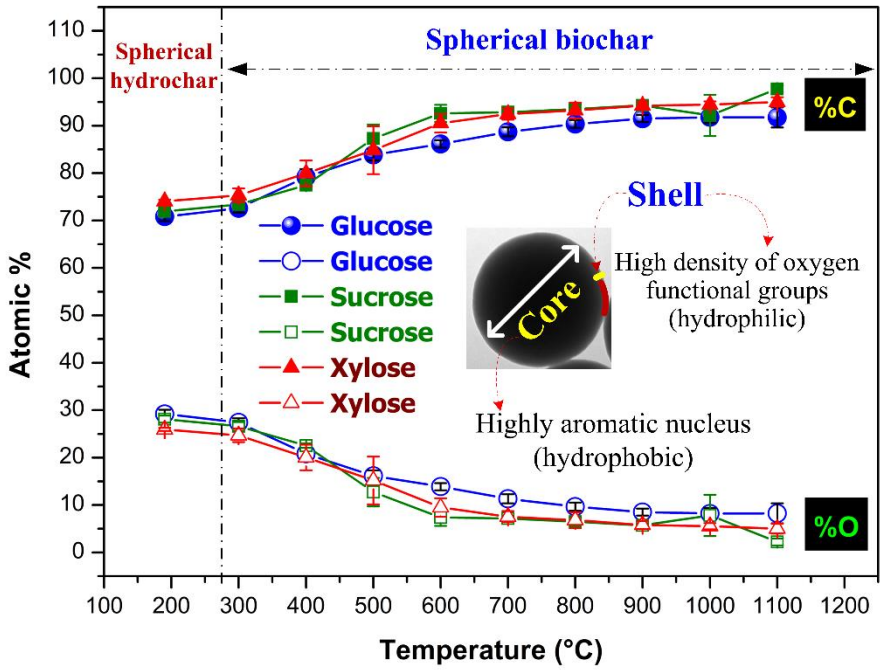

Figure 5. Effect of pyrolysis temperatures on main elements of spherical biocharsderived from glucose, sucrose, and xylose
(Data determined by EDX analysis; mean ± SD)

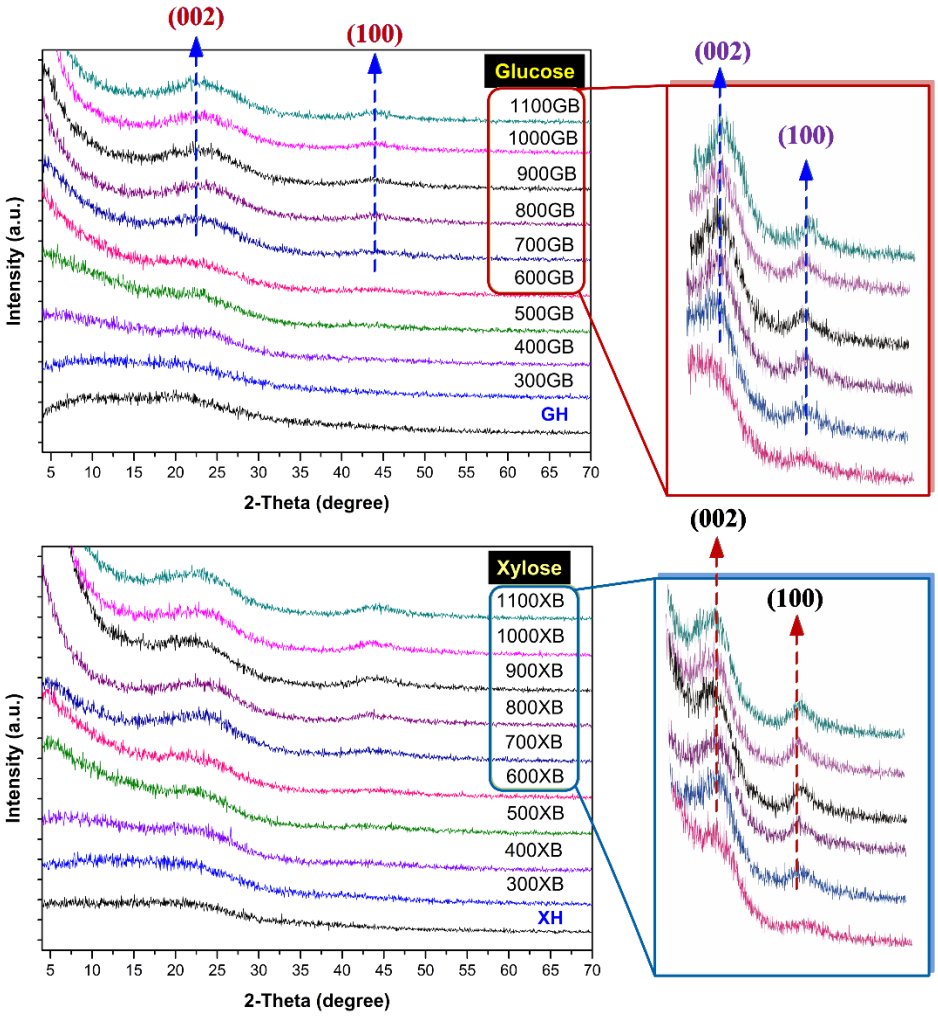

Figure 6. X-ray diffraction spectra of spherical biochars prepared at various pyrolysis temperatures and spherical hydrochars

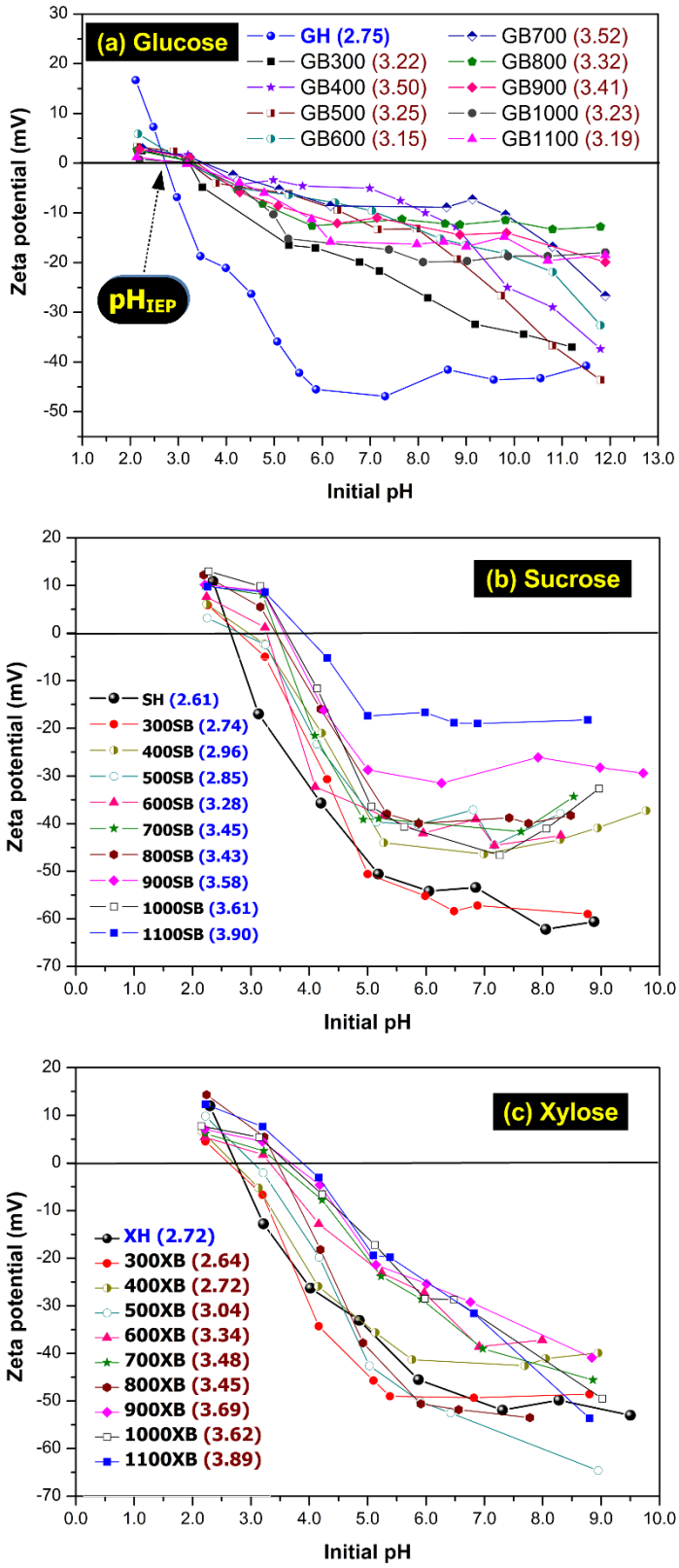

Figure 7. Dependence of zeta potential on pH for spherical biocharsderived from (a) glucose, (b)sucrose, and (c) xylose
(Digitals in parenthesis indicate values of isoelectric point; pH_{IEP})

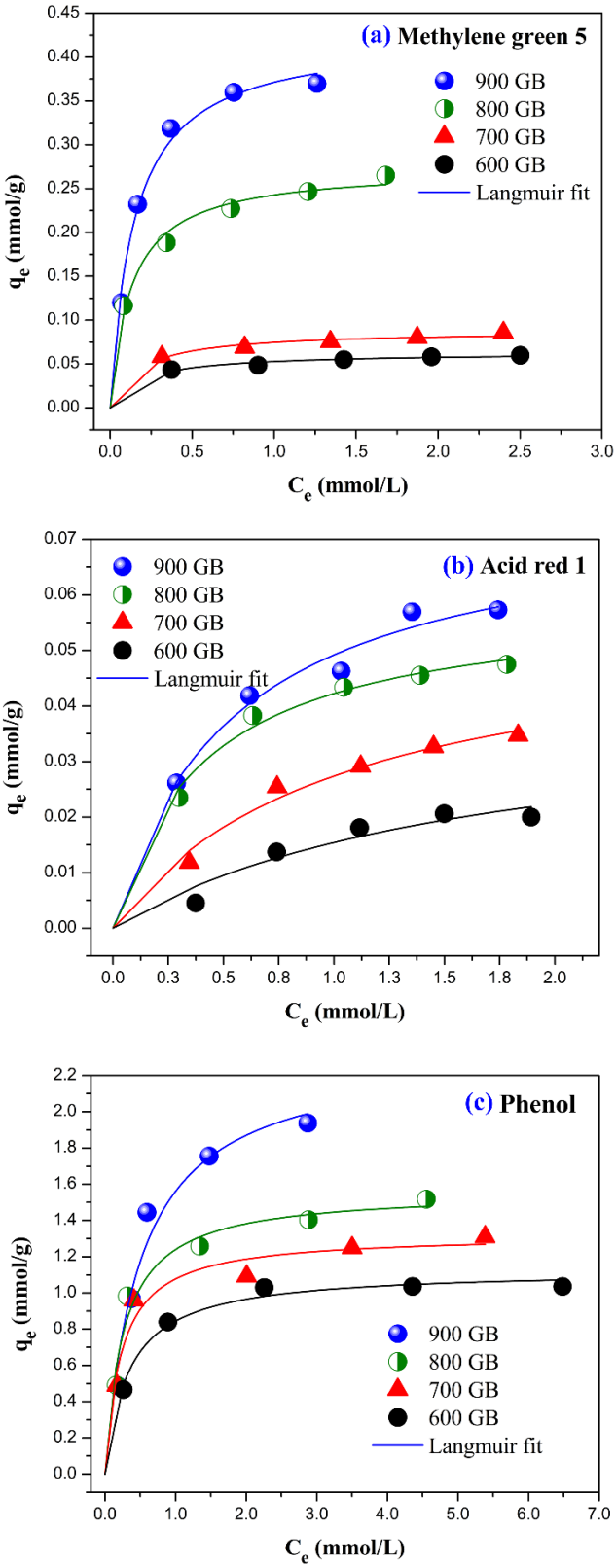

Figure 8. Adsorption isotherms of selected aromaticcontaminants onto glucose-derived sphericalbiochars prepared from different pyrolysis temperatures (600–900 °C).

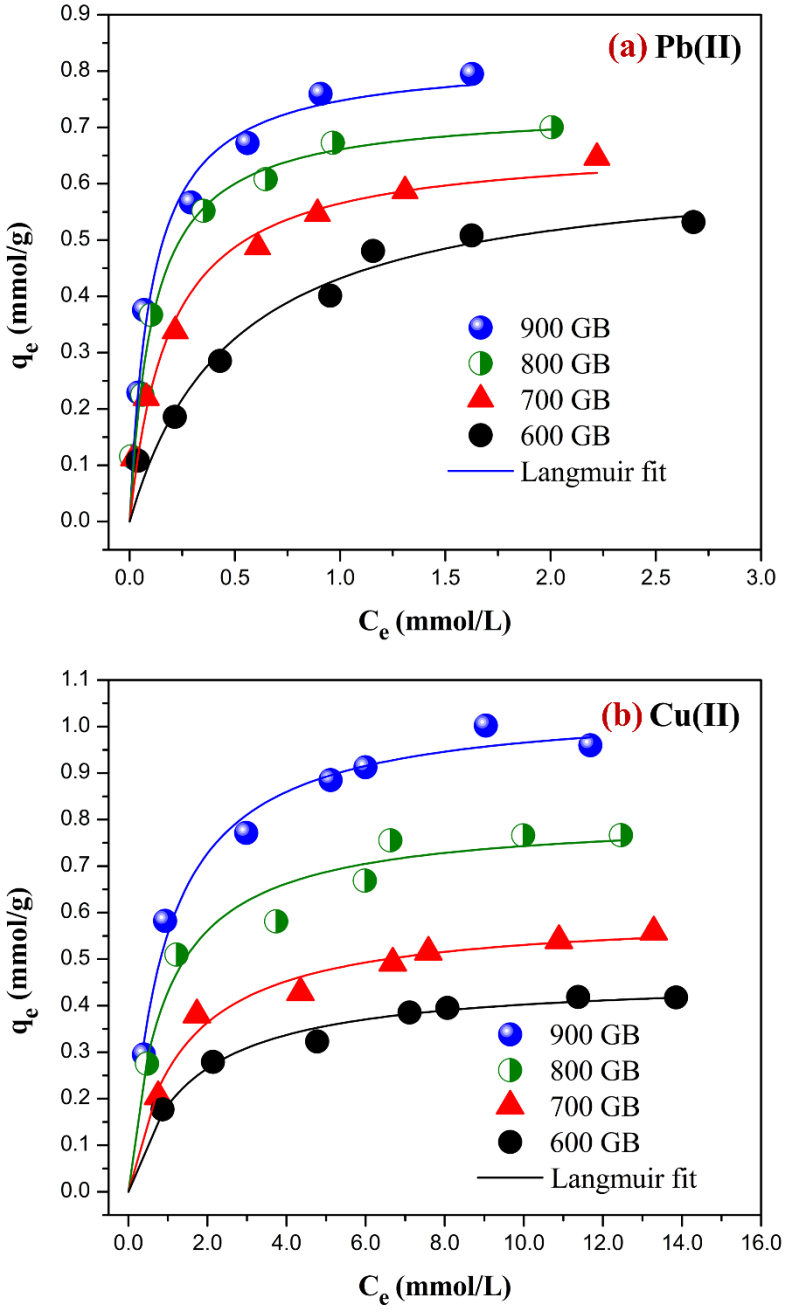

Figure 9. Adsorption isotherms of target heavy metals onto glucose-derived spherical biocharsprepared from different pyrolysis temperatures (600–900 °C).

Table 1. Textual parameters of the spherical hydrochar and biochar samples derived from glucose

	Surface area (m^2/g)				Pore volume (cm^3/g)		V_{Micro}/V_{Total}	L_o (nm)	E_o	Yield (%)
	S_{BET}	S_{Lang}	S_{Micro}	S_{Ext}	V_{Total}	V_{Micro}				
GH	7.08	9.79	–	–	0.008	–	–	–	–	42.5
300GB	13.8	17.8	8.2	5.6	0.013	0.004	30.8	3.77	14.3	–
350GB	35.5	42.2	a22.8	13	0.031	0.005	16.1	3.49	14.5	–
400GB	118	158	84.5	34	0.066	0.047	71.2	2.24	16.2	–
450GB	213	283	165	48	0.110	0.107	97.3	2.07	16.6	–
500GB	220	292	170	50	0.114	0.109	95.6	2.07	16.6	–
550GB	418	591	399	19	0.221	0.199	90.0	2.11	16.5	–
600GB	536	660	515	21	0.258	0.220	85.3	1.93	17.0	57.2
700GB	544	672	489	55	0.270	0.225	83.3	1.99	16.8	51.3
800GB	677	794	662	15	0.334	0.295	88.3	1.97	16.9	49.2
900GB	775	852	715	60	0.392	0.314	80.1	2.02	16.7	47.1
1000GB	484	677	477	7.0	0.246	0.236	95.9	2.03	16.7	–
1100GB	464	651	454	10	0.239	0.224	93.7	2.06	16.6	–
CAC[a]	768	–	–	–	0.430	0.219	50.9	2.24	16.2	–

Note: S_{BET} (BET surface area); S_{Lang} (Langmuir surface area); S_{Micro} (Micropore surface area); S_{Ext} (External surface area); V_{total} (total pore volume); V_{Micro} (micropore volume); L_o (average pore width); E_o (characteristic adsorption energy; kJ/mol); *yield* (%) calculated from the mass difference between before and after; and CAC[a] datapublished in our work (Huang, Lee et al. 2014).

Table 2. Textural parameters of the hydrochar and biochar samples derived from sucrose and xylose

	Surface area (m^2/g)				Pore volume (cm^3/g)		V_{mic}/ V_{toal}	L_o (nm)	E_o
	S_{BET}	S_{Lang}	S_{mic}	S_{ext}	V_{total}	V_{mic}			
Sucrose									
SH	0.985	2.53	—	—	0.003	—	—	—	—
300SB	6.823	10.5	—	—	0.004	—	—	—	—
400SB	7.807	11.0	—	—	0.009	—	—	—	—
500SB	409.5	581	395.6	13.9	0.212	0.197	93.1	2.07	16.62
600SB	406.2	571	399.5	6.7	0.205	0.198	96.8	2.01	16.76
700SB	398.9	558	396.5	2.4	0.198	0.196	98.9	1.99	16.83
800SB	389.9	544	363.7	26.2	0.191	0.178	93.0	1.96	16.90
900SB	407.2	587	372.0	35.2	0.207	0.190	91.8	2.04	16.70
1000SB	255.1	367	230.1	25.1	0.128	0.117	91.4	2.01	16.76
1100SB	159.8	230	148.2	11.6	0.080	0.076	95.1	1.99	16.82
Xylose									
XH	5.912	7.82	—	—	0.011	0.001	—	—	—
300XB	10.55	13.0	—	—	0.014	0.003	—	—	—
400XB	43.59	49.5	34.7	8.9	0.023	0.017	73.9	2.11	16.52
500XB	419.1	592	399.1	20.0	0.225	0.198	87.9	2.15	16.42
600XB	425.9	599	413.0	12.9	0.225	0.205	91.0	2.12	16.50
700XB	417.2	585	408.5	8.7	0.218	0.202	92.7	2.09	16.57
800XB	423.4	593	415.6	7.8	0.221	0.206	93.3	2.09	16.58
900XB	409.0	574	401.5	7.5	0.214	0.199	93.0	2.09	16.56
1000XB	348.0	501	313.4	34.7	0.191	0.160	83.7	2.19	16.33
1100SB	156.6	204	119.4	37.2	0.086	0.070	81.7	2.19	16.34

Note: S_{BET} (BET surface area); S_{Lang} (Langmuir surface area); S_{Micro} (Micropore surface area); S_{Ext} (External surface area); V_{total} (total pore volume); V_{Micro} (micropore volume); L_o(average pore width); E_o (characteristic adsorption energy; kJ/mol); *yield* (%) calculated from the mass difference between before and after.

Table 3. Corresponding isotherm parameters of the adsorptionof organic contaminants.

	Langmuir parameters				Freundlich parameters			ΔG°
	Q^{o}_{max} (mmol/g)	Q^{o}_{max} (mg/g)	K_L	R^2	K_F	n	R^2	
Methylene green 5								
GH	0.032	13.9	1.645	0.99	0.044	0.461	0.98	-28.8
600GB	0.065	28.3	3.656	0.91	0.051	0.180	0.98	-30.8
700GB	0.088	38.1	5.614	0.93	0.072	0.187	0.99	-31.9
800GB	0.274	119	7.798	0.97	0.237	0.254	0.98	-32.7
900GB	0.426	184	6.827	0.99	0.373	0.300	0.88	-32.4
CAC[a]	0.411	178	–	–	–	–	–	–
Acid red 1								
GH	0.042	21.2	1.476	0.96	0.023	0.421	0.97	-28.5
600GB	0.041	20.9	0.598	0.90	0.015	0.649	0.85	-26.2
700GB	0.056	28.2	0.973	0.97	0.026	0.536	0.93	-27.5
800GB	0.059	30.1	2.487	0.98	0.041	0.341	0.91	-29.8
900GB	0.076	38.6	1.843	0.97	0.047	0.412	0.95	-29.1
CAC[a]	0.253	129	–	–	–	–	–	–
Phenol								
GH	0.121	11.4	0.05	0.96	0.048	0.035	0.84	-20.0
600GB	1.127	106	2.99	0.98	0.774	0.199	0.82	-30.3
700GB	1.322	124	4.41	0.93	0.945	0.211	0.86	-31.3
800GB	1.562	147	3.85	0.95	1.088	0.243	0.88	-30.9
900GB	2.332	219	2.03	0.96	1.416	0.362	0.87	-29.3
CAC[a]	2.329	219	–	–	–	–	–	–

Note:the units of $\Delta G°$ (kJ/mol),K_L(L/mmol), and K_F[(mmol/g)/(mmol/L)^n];[a]data published in our previous work (Huang, Lee et al. 2014) with the same operating conditions.

Table4. Corresponding isotherm parameters of the adsorption of copper and lead.

	Langmuir parameters				Freundlich parameters			ΔG°
	Q^{o}_{max} (mmol/g)	Q^{o}_{max} (mg/g)	K_L	R^2	K_F	n	R^2	
Copper								
GH	0.291	60.3	0.79	0.97	0.126	0.473	0.97	-26.9
600GB	0.643	133	2.04	0.97	0.401	0.377	0.95	-29.3
700GB	0.673	140	5.2	0.98	0.533	0.317	0.98	-31.7
800GB	0.735	152	8.8	0.98	0.641	0.272	0.93	-33.0
900GB	0.825	171	9.63	0.99	0.748	0.311	0.93	-33.2
CAC[a]	0.121	25.1	–	–	–	–	–	–
Lead								
GH	0.396	25.2	0.371	0.98	0.162	0.272	0.86	-25.0
600GB	0.462	29.4	0.675	0.98	0.212	0.280	0.95	-26.5
700GB	0.599	38.1	0.773	0.97	0.253	0.277	0.94	-26.9
800GB	0.809	51.4	1.133	0.95	0.423	0.259	0.92	-27.8
900GB	1.052	66.8	1.122	0.98	0.539	0.273	0.92	-27.8
CAC[a]	0.657	41.8	–	–	–	–	–	–

Note:the units of ΔG° (kJ/mol), K_L (L/mmol), and K_F [(mmol/g)/(mmol/L)^n]; [a]data published in our previous work (Huang, Lee et al. 2014) with the same operating conditions.